Chapter 3

Subsurface Flow Fields of Sunspots[1]

3.1 Previous Observations

How plasma flows around a sunspot is an interesting topic that has been studied for decades. Measurements of the subsurface flow can help us to understand how sunspots form, grow, evolve, and decay. The Evershed effect is a well-known phenomenon, which is observed as a prominent outflow from the inner sunspot penumbra to its surrounding photosphere (Evershed, 1909). With the development of new technology to achieve better spatial and temporal resolution, more details of the Evershed effect have been disclosed. Recent results show that Evershed outflows concentrate mainly in narrow and elongated radial penumbral channels (Rimmele, 1995; Stanchfield et al., 1997). This may suggest that the Evershed effect is only a superficial phenomenon at the solar surface. More recent studies of vertical flows have found hot upflows in the inner penumbra, which feed the horizontal Evershed flow, and cool downflows surrounding the outer penumbra where the horizontal Evershed flow terminates (Schlichenmaier and Schmidt, 1999).

The studies mentioned above were conducted by direct spectral observations,

[1]Most part of this chapter was published in the Astrophysical Journal (Zhao, Kosovichev, & Duvall, 2001)

which cannot determine the material flow fields beneath the surface. Time-distance helioseismology provides a very useful technique to probe the interior structure and mass flows beneath the solar surface. Using the time-distance technique based on the travel time measurements of solar surface gravity waves (f mode), Gizon, Duvall, & Larsen (2000) detected a radial outflow, which has an average velocity of about 1 km s^{-1} in the top 2 Mm below the photosphere, extending from sunspot center to up to 30 Mm outside the sunspot umbra. Since the inferred outflow is significantly smaller than the surface outflow speed measured by Doppler velocity, they suggested the Evershed flow is very shallow, which is consistent with conclusions from direct spectral observations. Because of the surface nature of the f mode, these results can only reflect horizontal material motions in shallow layers just beneath the surface (Duvall & Gizon, 2000).

The origin of sunspots is not understood. Parker (1979) suggested a cluster model for sunspots. In order to hold together the loose cluster of magnetic flux tubes, a downdraft beneath the sunspot in the convection zone is needed. But so far, this model lacks direct observational evidence. Though Duvall et al. (1996) have obtained evidence for downflows under the sunspot by use of the time-distance technique, some authors (e.g., Woodard 1997; Lindsey et al. 1996) put this conclusion in suspicion.

In this chapter, we apply the time-distance technique based on measuring travel times of acoustic waves (p modes) to one set of continuous Dopplergram observations by SOHO/MDI. These travel times are inverted to probe the plasma flows under and around the sunspot region. The clear flow picture deep below and around the sunspot presented in this chapter provides strong support to the cluster sunspot model and emergence of magnetic Ω loops.

3.2 Data Acquisition

The set of data analyzed are high resolution Dopplergrams with one-minute cadence, obtained by MDI. The observations began at 15:37UT of June 18, 1998, and lasted for approximately 13 hours. A sunspot was at the center of the field of view and remained stable during the observation period. The resolution of observation is $0\overset{\circ}{.}034$/pixel, and

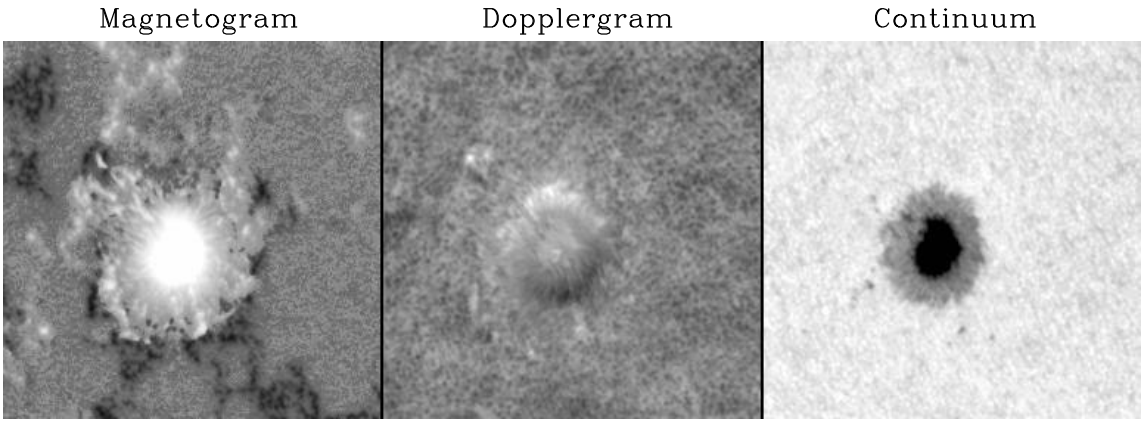

Figure 3.1: A magnetogram, Dopplergram and continuum graph of the studied sunspot in AR8243. The observation was obtained on June 18, 1998.

after a 2×2 rebin, we get an image of 256×256 pixels with resolution of 0.″068/pixel for each one-minute cadence. (Here, 1° represents 1 heliographic degree, which is approximately 12.15 Mm at disk center) A plot of a magnetogram, Dopplergram and intensity graph of the active region are presented in Figure 3.1.

After the dataset was tracked, remapped and filtered, time-distance measurements were then performed as described in §2.1 and Appendix A. To account for variations of the differential rotation with depth, the corresponding mean values of the differences from a quiet Sun region were subtracted from our travel-time differences.

3.3 Tests Using Artificial Data

Kosovichev (1996) applied an inversion technique used in geophysical seismic tomography to develop a new way to detect the mass flows and other inhomogeneities (e.g. sound speed variations) beneath the visible surface of the Sun. Detailed description of the method can be found in that paper. Equations relating flowing speed and travel time differences were solved by a regularized damped least-square technique (Paige & Saunders, 1982).

In order to check the spatial resolution of our calculation code, we designed some artificial data to simulate the flows in the solar interior. The travel time differences

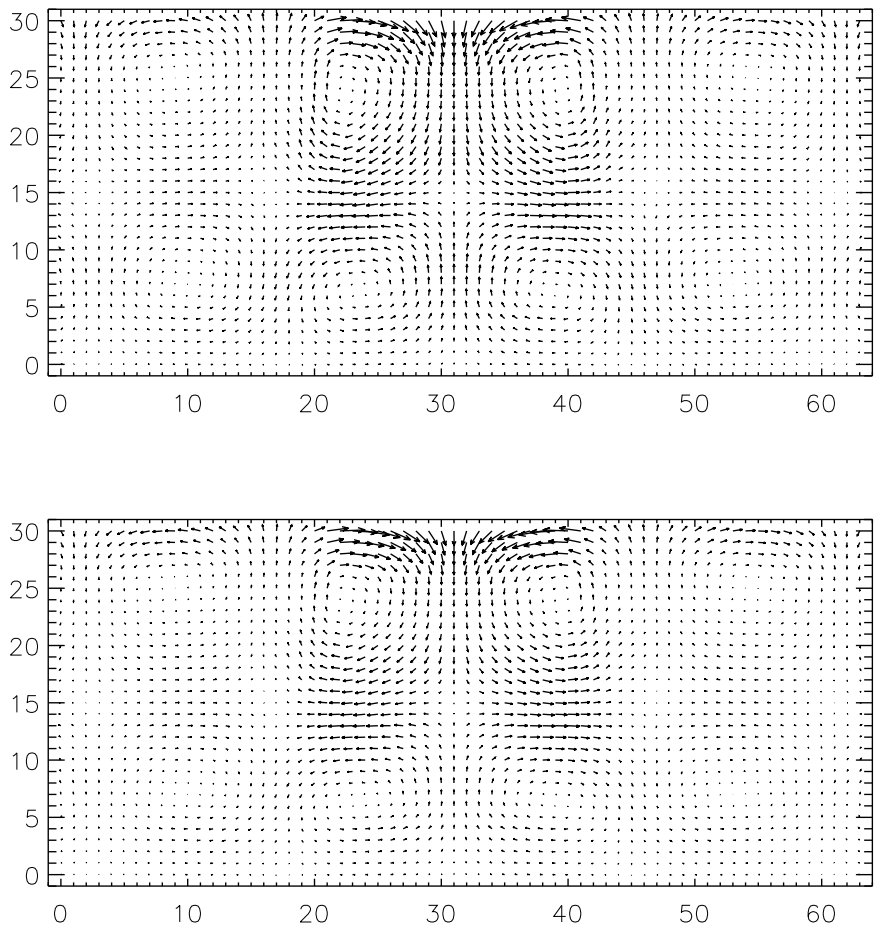

Figure 3.2: The experiment on our inversion code: *upper*, artificial data that simulates the flows of sunspots; *lower*, inversion results.

are calculated using a forward approach, then the inversion was done to get the flow speeds. We found that, generally, the flows in the upper layers can always be recovered well, but flows in the lowest layers may be smaller than the input values (see also Kosovichev and Duvall 1997). We also found that in some specific cases, because of a cross-talk between horizontal flows and vertical components of flow velocities, it may be impossible to recover the original data. This problem will be addressed again in more details in Chapter 6. However, for localized strong flows such as in sunspots, the cross-talk effects do not occur. Figure 3.2 shows a result from a set of our artificial data which has relatively strong motions in the central region. It can be found that

the flow patterns are recovered well, but the velocity magnitude in the lower layers is somewhat smaller than the input. Therefore, the inferred mass flow speeds in the upper layers of the sunspot region should be quite credible. In the lower layers these speeds are probably underestimated.

To double check our inversion results, we compute the travel time differences resulting from the velocities inferred from the inversion, which are compared with the travel time differences computed from time-distance analysis. These travel time differences were used to compute the flow velocities by inversion again to compare with the previous results. Good agreement was achieved from our calculations in both procedures. This means that the observational data are sufficient for recovering both the horizontal and vertical components of the velocities in the sunspot region.

3.4 Inversion Results

3.4.1 Subsurface Sound-speed Structure

Following the inversion technique in §2.3, and the artificial tests in last section, the inversions were performed on the real observational data of the sunspot.

The sound-speed variations below the sunspot's surface was obtained, as shown in Figure 3.3. It was found that about 3 Mm immediately below the sunspot's surface, the sound-speed variation is negative, perhaps due to the low temperature of plasma. Below 3 Mm, the sound-speed variations are largely positive and extend to approximately a depth of 20 Mm. It is yet not clear why the sound-speed is larger in these regions. The larger speed may result from a higher temperature of the plasma, or may result from the magetoacoustic speed that should be but was not disentangled from the sound-speed variations in the inversion procedure, as already discussed in §2.2.

The recent inversion efforts by use of Fresnel-zone approximation (Jensen et al., 2001; Couvidat et al., 2004) confirmed the sound-speed structures inverted here, with the similar structures and similar magnitude of variations. Different inversion codes with different choice of the regularization parameters are suspected to account for the

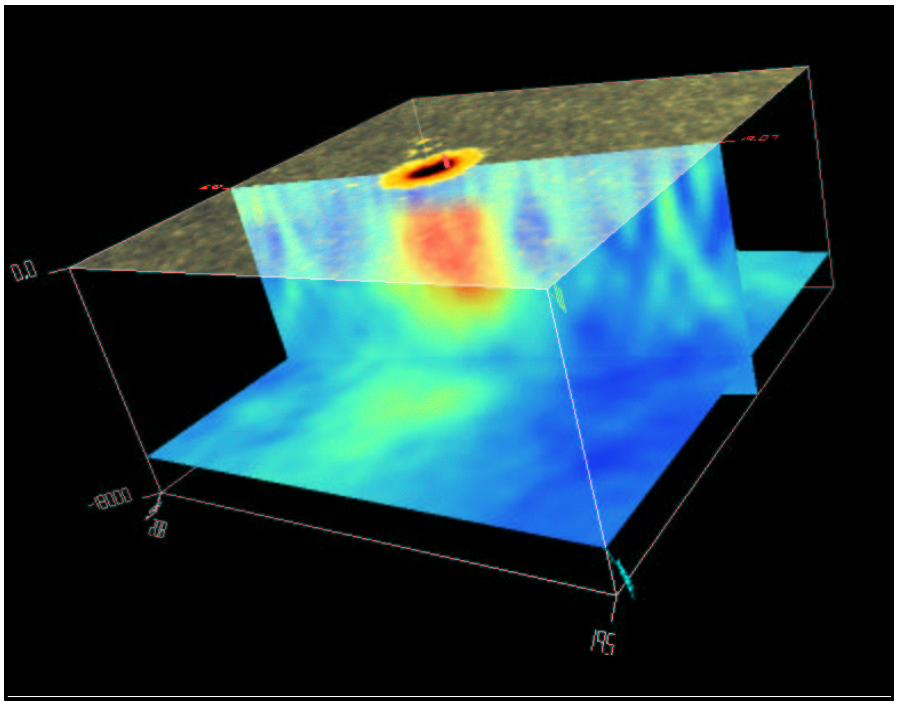

Figure 3.3: Sound-speed variations below the sunspot. The cold color (blue) represents negative sound-speed variations, and the warm color (yellow and red) represents positive variations (courtesy: SOHO/MDI).

slight differences.

3.4.2 Subsurface Flow Fields

We average the calculated travel time differences in 2×2 pixel rebin, thus obtain maps of 128×128 pixels for each $\delta\tau_{\rm oi}, \delta\tau_{\rm we}$ and $\delta\tau_{\rm ns}$ for the eleven different annulus ranges described in Appendix A. We adopt a ten-layer discrete model in depth of the sunspot region, and use the same number of pixels in each layer as in the time-distance measurements. The depth ranges for 10 layers are: 0–3, 3–4.5, 4.5–6, 6–9, 9–12, 12–14, 14–16, 16–18, 18–20.5 and 20.5–23 Mm. The results are presented in Figure 3.4 and Figure 3.5.

Figure 3.4 shows the mass flows in the first and the fourth layers, with arrows

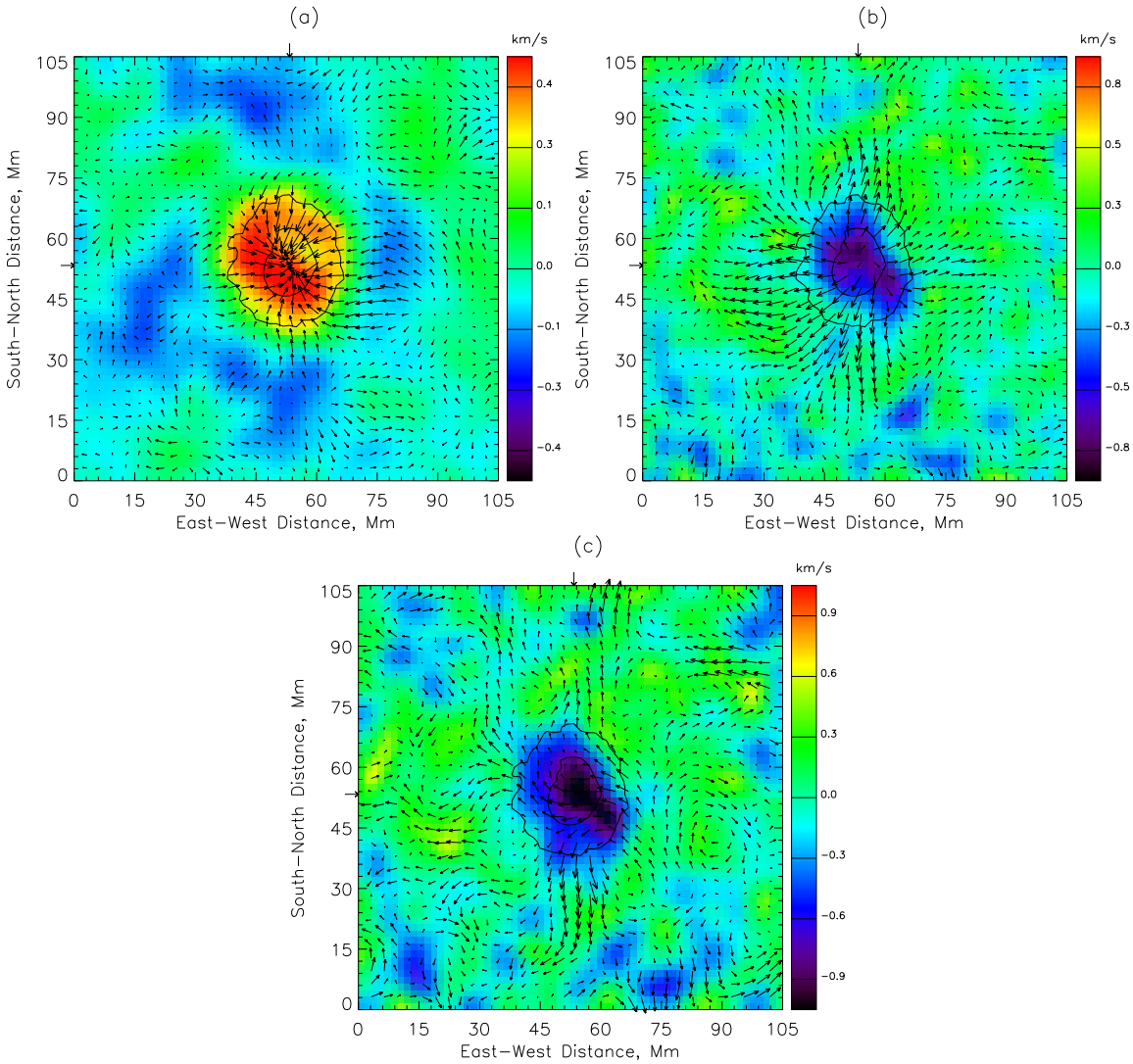

Figure 3.4: Flow fields at a depth of (a) 0 – 3 Mm, (b) 6 – 9 Mm and (c) 9 – 12 Mm. Arrows show magnitude and direction of horizontal flows, and the background shows vertical flows with positive as downward flows. The contours at the center correspond to the umbral and penumbral boundaries. The longest arrow represents 1.0 km/s for (a) and 1.6 km/s for (b) and (c). Arrows outside the frame indicate where the cut is made to obtain graphs of figure 3.5.

showing the direction and strength of the horizontal flows, and the background image showing the vertical velocities. From Figure 3.4a which shows results for the

first layer corresponding to an average of depth of 0–3 Mm, we can clearly identify a ring of strong downflows around the sunspot, with relatively weaker downflows inside the ring. Converging flows at the sunspot center can also be seen in this graph. Figure 3.4b shows the flows in the fourth layer, corresponding to a depth of 6–9 Mm. The sunspot region contains a ring of upflows with relatively smaller downward velocity at the center. Outside this region, the results are a little noisier, but downward velocities seem dominant in the region immediately outside the sunspot. Strong outflows from the sunspot center can be seen, extending more than 30 Mm from the sunspot center. Figure 3.4c shows the flows in the fifth layer, average of depth of 9–12 Mm, where powerful upflows occupy the whole sunspot region. It is of more interests to notice the horizontal mass flows in this layer. Some materials from the West flow right across the sunspot region, and continue moving mainly to the South-East quarter of the graph.

Figure 3.5 shows two vertical cut graphs, one in the East-West direction, the other in the North-South direction, through the center of the sunspot. Although the ten layers were calculated from observation, we only use the upper eight layers to provide more reliability to the results according to our test inversions. The velocities from inversion are actually the average velocities in the block. We assume these as the velocities at the center of the block, and also assume the velocities change uniformly from the block to its neighboring blocks, and calculate the speeds in between two layers by use of linear interpolation. Converging and downward flows can be seen in both graphs right below the sunspot region from 1.5 Mm to about 5 Mm. Below that, the horizontal outflows seem to dominate in this region, though relatively weaker upflows also appear. Below a depth of $\sim$10 Mm, the flows seem not to be concentrated in the region vertically below the sunspot. This can be seen more clearly in the East-West cut. It is intriguing that an upflow towards the East dominates in the region from 10 Mm to 18 Mm. In the South-North cut graph, this pattern is not so clear but still can be seen, with the upflow towards the South stronger than towards the North.

In order to check whether the velocity distribution can keep the structure stable or quasi-steady, $\nabla \cdot (\rho \mathbf{v})/\rho$ was computed, where ρ is the density from a standard

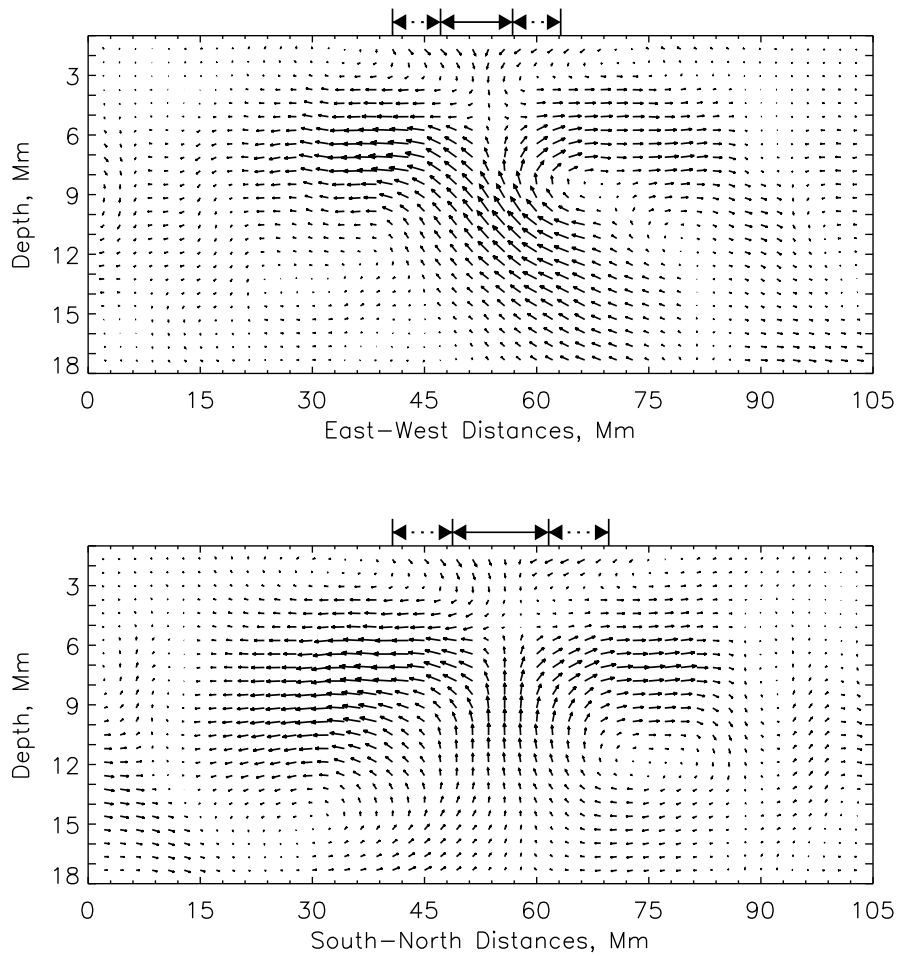

Figure 3.5: Vertical cuts through the sunspot center, with a cut direction of East-West (*upper*, east on left side) and South-North (*lower*, south on left side). The range covered by the line arrow indicates the area of the umbra, and the range covered by the dotted arrow indicates the area of penumbra. The longest arrow indicates a velocity of 1.4 km/s.

solar model. The largest value is of order 10^{-4} s^{-1}, slightly larger than the inverse of the duration of observation. However, the density distribution inside the sunspot and around it, where the magnetic field should be significantly large and the temperature obviously low, is probably significantly different from the standard model, and remains to be determined. Therefore, it is quite possible that the velocity distribution shown in the graph is consistent with the sunspot structure.

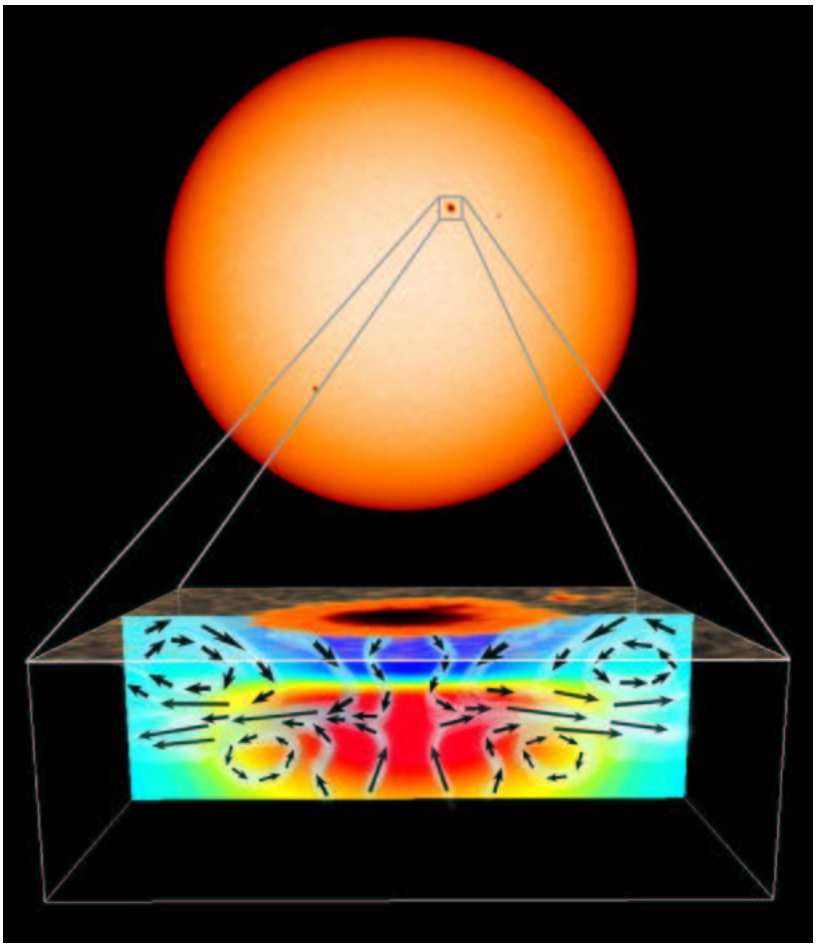

Figure 3.6: A cartoon showing both the sound-speed variations and the subsurface flow patterns of a sunspot (Courtesy: *SOHO*/MDI).

3.5 Discussion

We have presented our best estimates of the flows associated with a sunspot, and believe that these provide an accurate qualitative description of the flow pattern. Several factors could affect the accuracy of our results. It is unavoidable to have averaging effects between neighboring pixels and neighboring layers in our calculations. So, the flow speeds shown in Figures 3.4 and 3.5 can not represent the exact magnitudes, directions or locations, but some average values with their neighboring pixels and layers. Also, we have to bear in mind that the flows shown in Figures 3.4

and 3.5 are averages of 13 hours of observation. That means our inferences can only reflect flow patterns that are stable for a long time run rather than instantaneous speed at any observation time.

In our calculation, we assume that the travel time differences from time-distance analysis are totally due to mass flows, and we employ the geometrical ray approximation. Woodard (1997) and Birch & Kosovichev (2000) argued that some other factors, such as non-uniform distributions of acoustic sources and finite wavelength effects, may also affect travel times, which may greatly complicate our analysis, in particular, quantitative inferences.

In both graphs of Figure 3.5, powerful converging and downward flows are found from 1.5 Mm to ∼5 Mm beneath the surface. Meyer et al. (1974) predicted the existence of the converging flow (∼1 km/s at a depth of several Mm) as a collar

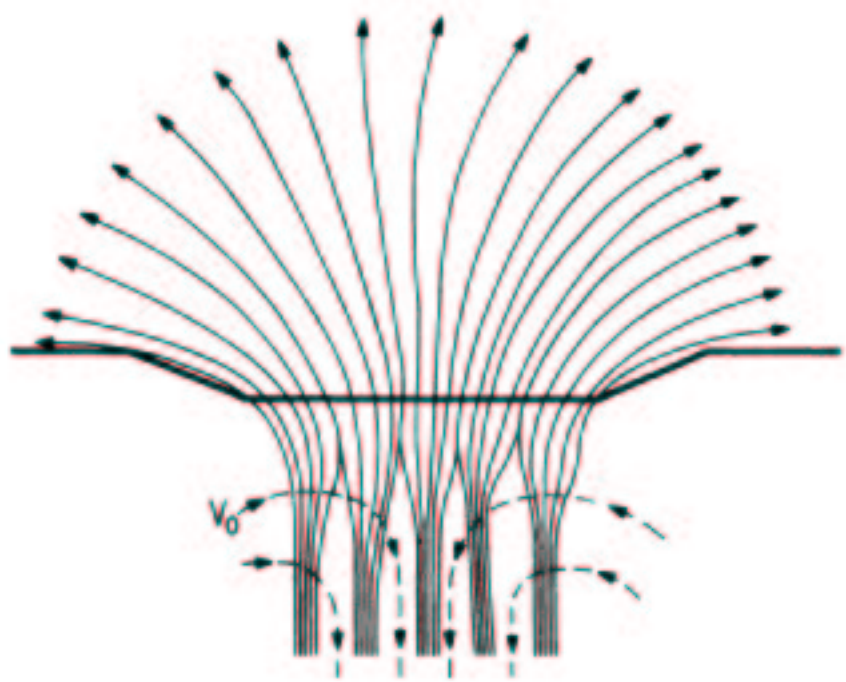

Figure 3.7: The cluster model of sunspots proposed by Parker (1979). This plot is adopted from that paper.

around the sunspot to provide the confinement and stability of sunspots. The material downdrafts below the sunspot were also required to keep the cluster of magnetic fluxes confined under the sunspot in the cluster sunspot model (Parker, 1979), as shown in Figure 3.7. Our observation seems to have provided strong evidence for both predictions. More recent numerical simulations (Hurlburt & Rucklidge, 2000) show in more detail the converging and downward flows below the sunspot surface, and the upflow near the moat, which are in good agreement with our observation not only in the converging and downward flows, but also in upflows near the moat (a little weaker in our results than the simulation). The converging and downward flow beneath the sunspot cannot be immediately consistent with the other observed facts of upward and diverging flows at the surface, as described in §3.1. Further studies of the shallow region from the surface to a depth of 2 Mm should be done more carefully by combining the f mode observations (Gizon, Duvall, & Larsen, 2000).

Besides the cluster model, the monolithic model is another widely proposed sunspot model. It suggests that the sunspot is one large magnetic flux tube below the photosphere rather than dividing into some small flux tubes. If this is true, one should expect no material can flow across the monolithic magnetic tube. But our results in Figure 3.4c shows otherwise. This may be a further evidence to support the cluster model, which does not prohibit mass flow across the lower part of a sunspot.

It is clear that magnetic inhibition of convection is most effective within 1.5 Mm of the photosphere (Thomas and Weiss, 1992). The temperature difference, ΔT, between the sunspot umbra and the mean undisturbed atmosphere at the level of the Wilson depression is about 900K, but ΔT decreases rapidly with depth. The estimated value of ΔT falls to 500K at depth of 2 Mm, and then to 25K at depth of 6 Mm (Meyer et al., 1974). The sunspot would be a shallow phenomenon if it were defined by its thermal properties alone. Our calculation of flows shows that converging and downward flows disappear below the depth of $\sim$5 Mm, which is an approximate depth where ΔT vanishes. So, it may be interpreted that, the converging and downward flows beneath the sunspot are phenomena related to the sunspot's thermal properties. These flows disappear as the temperature difference of the sunspot with its surroundings vanishes.

It is widely believed that a sunspot is formed when the magnetic Ω loop rises from

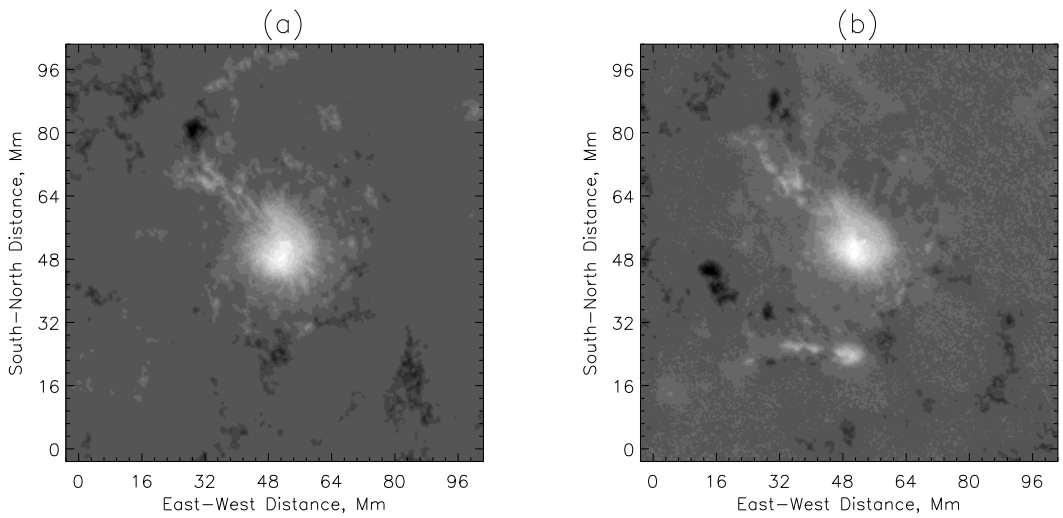

Figure 3.8: Magnetograms taken by MDI at (a) 04:30UT and (b) 22:00UT on June 19, 1998.

the deeper convection zone and emerges at the solar surface. The sunspot is located where the Ω loop emerges and where strong magnetic flux bundles concentrate. The flux bundles will stop rising after the sunspot reaches its maximum, but plenty of other magnetic flux keeps rising from the convection zone at the local site (Parker, 1994). There must be plenty of magnetic flux tubes which are underlying the sunspot but do not emerge on the surface despite of magnetic buoyancy. Figure 3.4c shows a strong mass flow across the sunspot, if some magnetic flux tubes underlying the spot are blown away to the South-East of the sunspot, and brought up by some upflows (some strong upflows can be found at the lower left corner of Figure 3.4c), magnetic emergence at the surface will be expected after ∼4 hours (from a depth of 9–12 Mm, the rising speed is around 0.7 km/s). We checked MDI full-disk magnetograms, and found about 5 hours after our analysis period, at 09:40UT of June 19, a magnetic emergence was first seen at the exact site of the upflows seen in Figure 3.4c. The pores with opposite polarities developed into their maxima after 12 hours. Figure 3.8 shows the magnetogram before the magnetic emergence and after it reaches the maximum. The sound-speed perturbation analysis of the same sunspot by Kosovichev, Duvall, & Scherrer (2000) revealed that the sunspot is connected with the pore of same

polarity in the deep interior, which may confirm our assumption that these two newly emerged pores were formed by rising Ω loops which might have broken away from the main magnetic flux bundles. We have also noticed another fact that the proper motion of this sunspot during the observation is towards the South-East. It may be caused by the South-East directed motion of the lower portion of the sunspot seen in Figure 3.4c due to an unknown reason. Obviously, more high-resolution helioseismic observations are required to confirm these results. Such observations could offer a unique opportunity for solving one of the great puzzles of astrophysics − the origin of sunspots.